# Mode of Cell Death Induction by Pharmacological Vacuolar H<sup>+</sup>-ATPase (V-ATPase) Inhibition\*<sup>S</sup>

Received for publication, August 20, 2012, and in revised form, November 11, 2012 Published, JBC Papers in Press, November 20, 2012, DOI 10.1074/jbc.M112.412007

Karin von Schwarzenberg<sup>‡1</sup>, Romina M. Wiedmann<sup>‡</sup>, Prajakta Oak<sup>§</sup>, Sabine Schulz<sup>¶</sup>, Hans Zischka<sup>¶</sup>, Gerhard Wanner, Thomas Efferth\*\*, Dirk Trauner\*\*, and Angelika M. Vollmar\*

From the <sup>‡</sup>Department of Pharmacy, Pharmaceutical Biology, Ludwig-Maximilians-University, 81377 Munich, Germany, the  $^\S$ Department of Pharmacy, Pharmaceutical Biology-Biotechnology, Ludwig-Maximilians-University, 81377 Munich, Germany, the  $^{\P}$ Institute of Toxicology, Helmholtz Center Munich, German Research Center for Environmental Health, 80539 Neuherberg, Germany, the  $^{\parallel}$ Department of Biology I, Ludwig-Maximilians-University, 81377 Munich, Germany, the \*\*Department of Pharmaceutical Biology, Institute of Pharmacy and Biochemistry, University of Mainz, 55099 Mainz, Germany, and the <sup>‡‡</sup>Department of Chemistry, Ludwig-Maximilians-University, 81377 Munich, Germany

Background: V-ATPase is proposed as tumor target, but information on cell death-inducing mechanisms is rare.

**Results:** Cell death induced by the V-ATPase inhibitor archazolid involves the cellular stress response.

**Conclusion:** Archazolid is a chemical tool to decipher V-ATPase-related cell death signaling.

Significance: Understanding the mechanism of V-ATPase inhibition-induced apoptosis is crucial to understand the impact of V-ATPase inhibition in cancer treatment.

The vacuolar H<sup>+</sup>-ATPase (V-ATPase), a multisubunit proton pump, has come into focus as an attractive target in cancer invasion. However, little is known about the role of V-ATPase in cell death, and especially the underlying mechanisms remain mostly unknown. We used the myxobacterial macrolide archazolid B, a potent inhibitor of the V-ATPase, as an experimental drug as well as a chemical tool to decipher V-ATPase-related cell death signaling. We found that archazolid induced apoptosis in highly invasive tumor cells at nanomolar concentrations which was executed by the mitochondrial pathway. Prior to apoptosis induction archazolid led to the activation of a cellular stress response including activation of the hypoxia-inducible factor- $1\alpha$  (HIF1 $\alpha$ ) and autophagy. Autophagy, which was demonstrated by degradation of p62 or fusion of autophagosomes with lysosomes, was induced at low concentrations of archazolid that not yet increase pH in lysosomes. HIF1 $\alpha$  was induced due to energy stress shown by a decline of the ATP level and followed by a shutdown of energy-consuming processes. As silencing HIF1 $\alpha$  increases apoptosis, the cellular stress response was suggested to be a survival mechanism. We conclude that archazolid leads to energy stress which activates adaptive mechanisms like autophagy mediated by HIF1 $\alpha$  and finally leads to apoptosis. We propose V-ATPase as a promising drugable target in cancer therapy caught up at the interplay of apoptosis, autophagy, and cellular/metabolic stress.

Vacuolar H<sup>+</sup> ATPase (V-ATPase)<sup>2</sup> is a complex multisubunit enzyme that translocates protons from the cytoplasm into intracellular compartments and across the plasma membrane. V-ATPases consist of a transmembrane V<sub>0</sub> complex responsible for proton translocation and a cytoplasmatic V<sub>1</sub> complex that hydrolyzes ATP. By regulating cellular pH homeostasis the V-ATPase is involved in a variety of cellular functions such as receptor-mediated endocytosis or activation of proteases (1). Tumor cells are often forced to exist in a hypoxic and acidic microenvironment due to low O2 and nutrient supply leading to increased glycolysis. Augmented expression of V-ATPase is considered to be a well designed compensatory mechanism which in fact confers survival and growth advantages of cancer cells (1, 2).

Thus, inhibitors of V-ATPases could be promising novel therapeutics for cancer. Most of the known V-ATPase inhibitors are natural compounds of microbial origin such as bafilomycin, the first specific inhibitor isolated from *Streptomyces* griseus in the 1980s. The family of specific V-ATPase inhibitors is still rather small but extensively studied regarding their binding properties and their mode of inhibition of V-ATPase as reviewed by Huss et al. (3).

Archazolid B, a macrolide originally produced by the myxobacterium Archangium gephyra, but also accessible by chemical synthesis (4, 5), attracted much attention being a highly specific and potent V-ATPase inhibitor. It binds within the equatorial region of the  $V_0$  rotor subunit c (6). There are reports on effects of V-ATPase inhibitors including archazolid on tumor growth and invasion (7-9); however, detailed investigations into the underlying molecular mechanism and signaling pathways are missing. In this respect archazolid could serve as a helpful pharmacological tool to decipher the role of V-ATPase in cell death

inducible factor-1α; HMEC, human mammary endothelial cell; HUVEC, human umbilical vein endothelial cell; JC-1, 5,5',6,6'-tetrachloro-1,1',3,3'tetraethylbenzimidazol-carbocyanine iodide; 3MA, 3-methyladenine; mTOR, mammalian target of rapamycin; NBDG, 2-[N-(7-nitrobenz-2-oxa-1,3-diazol-4-yl)amino]-2-deoxy-D-glucose; TES, N-tris(hydroxymethyl)methyl-2-aminoethanesulfonic acid.



<sup>\*</sup> This work was supported by the Deutsche Forschungsgemeinschaft Grant FOR 1406 Vo 376/15-1.

This article contains supplemental Figs. 1S–5S, Materials and Methods, and additional references.

<sup>&</sup>lt;sup>1</sup> To whom correspondence should be addressed: Dept. of Pharmacy, Pharmaceutical Biology, LMU Munich, Butenandtstrasse 5-13, 81377 Munich, Germany. Tel.: 0049-89-218077165; Fax: 0049-89-218077170; E-mail: karin.von.schwarzenberg@cup.uni-muenchen.de.

<sup>&</sup>lt;sup>2</sup>The abbreviations used are: V-ATPase, vacuolar H<sup>+</sup> ATPase; AMPK, AMPactivated protein kinase;  $\Delta \psi$ m, mitochondrial potential; HIF1 $\alpha$ , hypoxia-

mechanisms of tumor cells which has not been addressed in detail up until now.

Killing tumor cells by chemotherapeutic agents is frequently associated with enhanced cellular stress. A cellular stress response can be induced by disturbance of the cellular homeostasis or by a variety of stressful stimuli like chemotherapeutics, starvation, hypoxia, or DNA damage. To escape this stress and survive, tumor cells evolve adaptive mechanisms via activating prosurvival and/or antiapoptotic pathways. However, if cellular stress is severe enough the apoptotic machinery will be activated (10, 11).

One major player in cellular stress response is the BH-3 only protein BNIP3. It was first discovered in a yeast two-hybrid screen for proteins that interact with the adenovirus E1B 19 kDa, a homolog of Bcl-2, and is described to have pro- and antiapoptotic effects depending on the cell type and the stimuli (12). Its major inducer is the hypoxia-inducible factor- $1\alpha$  (HIF1 $\alpha$ ), which is the main activator of hypoxic stress responses and can induce autophagy (13).

The role of autophagy in cancer is rather complex. Autophagy is a highly regulated process of degradation and recycling of proteins in response to starvation and stress. It is characterized by the formation of double membrane autophagosomes that fuse with lysosomes in which proteins are degraded and recycled. Autophagy is mostly considered to serve as a cell survival pathway to suppress apoptosis. However, persistent autophagy can lead to cell death (14-16).

The transcription factor HIF1 $\alpha$  is another important player in cellular stress response. It consists of an oxygen-sensitive  $\alpha$ -subunit and a constitutive expressed  $\beta$ -subunit and is mostly regulated by proteasomal degradation (17).

In hypoxia, HIF1 $\alpha$  degradation is inhibited, and the protein is able to activate >100 genes involved in glycolysis or angiogenesis supporting tumor growth. However, prolonged activation of HIF1 $\alpha$  can lead to proapoptotic processes due to an accumulation of lactic acid mediated either by activation of p53 or the mitochondrial pathway of apoptosis (18, 19).

The aim of this study was to decipher the mechanism of pharmacological inhibition of V-ATPase leading to tumor cell death. We show that archazolid B, a novel V-ATPase inhibitor, induces a cellular stress response that is mediated by HIF1 $\alpha$ , involves autophagy, and finally leads to apoptosis of cancer cells. This work suggests that V-ATPase is a promising drugable target at the interplay of tumor cell metabolism, autophagy, and apoptotic processes.

#### **EXPERIMENTAL PROCEDURES**

Cell Lines and Reagents—The human breast cancer cell line SKBR3 was kindly provided by Dr. Barbara Meyer, and the pancreatic tumor cell line L3.6pl was a gift from Dr. Christiane Bruns (Department of Surgery, Klinikum Grosshadern, LMU Munich). HEK292 cells were purchased from DMSZ (Braunschweig, Germany). HUVECs were bought from PromoCell (Heidelberg, Germany), and HMECs were from CDC (Atlanta, GA). MDA-MB-231, MCF-7, and L929 cells and the human mammary epithelial cell line MCF10A were purchased from ATCC and 4T1-Luc2 mouse breast carcinoma cells were purchased from Caliper Life Science (Alameda, CA). SKBR3 cells

were cultured in McCoy's 5A medium supplemented with 10% FCS and 1% glutamine. MCF10A cells were cultured in DMEM-F12 supplemented with 5% horse serum, 100 mg/ml epidermal growth factor, 10 mg/ml insulin, 1 mg/ml hydrocortisone, 1 mg/ml cholera toxin, and penicillin/streptomycin. HUVECs and HMECs were cultured in endothelial growth medium (PromoCell) containing 10% FCS and a supplemental mix of vitamins and growth factors (PromoCell). All other cell lines were grown in RPMI 1640 medium containing 10% FCS. All cells were grown at 37 °C, 5% CO<sub>2</sub>. All media were purchased from PAA Laboratories (Pasching, Austria). Archazolid B was synthesized by Prof. Dirk Trauner (4) (Department of Chemistry, LMU Munich), 3-methyladenine was from Calbiochem, QVD-Oph was purchased from R&D Systems, and concanamycin A was from Enzo Life Science (Loerrach, Germany).

Cell Viability Assays—Subdiploid DNA content was determined as described (20) and analyzed by flow cytometry (BD Biosciences). Subdiploid cells left of the  $G_1$  peak were considered apoptotic.

Chromatin condensation was analyzed by Hoechst staining. After treatment, nuclei were stained with 0.5  $\mu$ g/ml Hoechst 33258 (Sigma-Aldrich) for 5 min and analyzed by fluorescence microscopy. Growth inhibition was measured with the CellTiter-Blue Assay (Promega) according to the manufacturer's instructions.

Cell Proliferation—1500 cells/well were seeded into 96-well plates and allowed to adhere overnight. To determine the initial amount of cells, control cells were fixed and stained with crystal violet. Cells were incubated with the indicated doses for 72 h and subsequently stained with crystal violet (0.5% crystal violet in 20% methanol). The absorbance at 550 nm was measured in a Sunrise ELISA reader (Tecan, Maennerdorf, Austria) and is proportional to the cell number.

Clonogenic Assay—Cells were treated as indicated for 24 h, trypsinized, and counted, and the volume of  $5 \times 10^3$  cells was plated into 6-well plates in triplicate. After an incubation time of 7 days, cells were stained with crystal violet (0.5% crystal violet in 20% methanol). The absorbance of crystal violet was measured at 550 nm with a Sunrise ELISA reader (Tecan).

Bax Activation—Bax activation was measured as described previously (21). Briefly, after treatment, cells were harvested, fixed with 0.5% paraformaldehyde, and stained with 0.5  $\mu$ g of anti-Bax 6A7 antibody (BD Biosciences). After washing, cells were stained with an Alexa Fluor 488-labeled goat anti-mouse antibody (Molecular Probes) 1:400, and conformational change of Bax was measured by flow cytometry.

Cytochrome c Release—Cytochrome c release was measured according to Waterhouse and Trapani (22). Briefly, SKBR3 cells were incubated as indicated, harvested, and permeabilized in a digitonin-containing buffer (100 mm KCl, 50  $\mu$ g/ml digitonin in PBS). After washing, cells were fixed with 4% paraformaldehyde. Next, cells were incubated with a cytochrome c antibody (Cell Signaling Technology) overnight at 4 °C. After two washing steps cells were incubated with an Alexa Fluor 488-labeled goat anti-rabbit secondary antibody (Molecular Probes) and then analyzed immediately by flow cytometry.

*Isolation of Rat Liver Mitochondria*—Mitochondria were isolated from freshly removed rat liver tissue by differential cen-



trifugation and further purified by Percoll density gradient centrifugation essentially as described (23). Organelles were washed twice (9000  $\times$  g, 4 °C, 10 min) and resuspended in isolation buffer (5 mm TES, 300 mm sucrose, 0.2 mm EGTA, 0.1% BSA, pH 7.2 with KOH).

Mitochondrial Potential ( $\Delta \psi m$ )—Cells were treated as indicated. After harvesting, cells were stained with JC-1 (Alexis Biochemicals, Loerrach, Germany) at a final concentration of 1.25 μM for 30 min at 37 °C and analyzed by flow cytometry. JC-1 forms red fluorescent aggregates in healthy mitochondria. When the mitochondrial potential decreases, JC-1 stays in its monomeric form leading to green fluorescence.

 $\Delta \psi$ m in isolated rat liver mitochondria was measured by the rhodamine-123 quenching method as described (24). Measurements were done in duplicate for 60 min in a microplate fluorescence reader (excitation 485/20, emission 528/20; BioTEK, Bad Friedrichshall, Germany).

Caspase Activity—Caspase activity was analyzed as described previously (25). The caspase substrates DEVD-AFC (caspase-3) or LEHD-AFC (caspase-9), both from Oncogene Research Products, were used. Caspase activity was monitored by a platereading multifunction photometer (Tecan) after 2 h at 37 °C. Activity was normalized to the protein concentration.

ATP Assay—SKBR3 cells were seeded in a 96-well plate and treated as indicated. ATP level was determined using the Cell-Titer-Glo assay (Promega) according to the manufacturer's instructions and measured in a luminometer (Berthold Technologies, Bad Wildbad, Germany).

Immunoblotting-Protein lysis, nuclear extraction, and immunoprecipitation were performed as described before (21). For fractioning of mitochondrial membranes a digitonin-containing buffer was used. Equal amounts of protein were separated on a SDS-PAGE and transferred to a nitrocellulose membrane. The membranes were blocked with 5% milkpowder and then probed with primary antibodies.

The following antibodies were used: PARP-1 (Oncogene Research Products), caspase-3, LC3I/II, p-AMPK, AMPK, p-eiF2 $\alpha$ , beclin-1, Bcl-X<sub>L</sub>, p62 (Cell Signaling Technology), eiF2α, ATG5 (Santa Cruz Biotechnology, Santa Cruz, CA),  $HIF1\alpha$  (BD Biosciences), BNIP3 (Abcam), actin (Chemicon), HRP-goat anti-rabbit (Bio-Rad), HRP-goat anti-mouse (Santa Cruz Biotechnology).

Confocal Microscopy—Cells were treated as indicated, fixed with 4% paraformaldehyde for 20 min, permeabilized with 0.1% Triton X-100, and blocked with 2% BSA. The primary and secondary antibody were diluted in 2% BSA and incubated for 1 h. Finally, cells were mounted with PermaFluor<sup>TM</sup> mounting medium (Beckman Coulter) and analyzed with a Zeiss LSM 510 Meta confocal microscope (Jena, Germany).

The following antibodies or staining were used: Lamp-1 (Developmental Studies Hybridoma Bank Iowa), rhodaminephalloidin (Invitrogen), Hoechst 33258 (Sigma-Aldrich), BNIP3 (Abcam), Alexa Fluor 633-goat anti-mouse, Alexa Fluor 546-goat anti-mouse (Molecular Probes). For monitoring mitochondria with a MitoTracker (Molecular Probes), cells were treated as indicated, and the manufacturer's protocol was followed.

LysoTracker—For monitoring the pH of lysosomes with a LysoTracker (Molecular Probes) cells were either stained for 30 min and analyzed by confocal microscopy or harvested, stained for 30 min at 37 °C, and analyzed by flow cytometry.

Glucose Uptake-Cells were treated as indicated. Subsequently cells were incubated with 100  $\mu$ M 2-NBDG (Invitrogen) in Hanks' buffer for 30 min at 37 °C. Then cells were harvested, and changes in glucose uptake were measured by flow cytometry.

Cell Transfection—ATG5, BNIP3, and HIF1 $\alpha$  were silenced using ON-TARGET-Plus SMARTpool siRNA (2 µg) from Dharmacon and nontargeting siRNA as a control.  $1 \times 10^6$ SKBR3 cells were transfected using the Amaxa Nucleofector kit V (Lonza, Ratingen, Germany), program A-23, according to the manufacturer's instructions and were treated as indicated 24 h after transfection. EGFP-LC3 plasmid (Addgene) was transfected (2 μg) using the FuGENE kit (Roche Applied Science) according to the manufacturer's protocol.

Spheroids-40,000 SKBR3 cells/ml were seeded in poly-HEMA (50 mg/ml) (Sigma-Aldrich) coated plates and grown for 7 days. Half of the spheroids was trypsinized into single cells followed by counting the amount required to seed 5000 cells/ well and accordingly whole mammospheres were seeded in polyHEMA-coated 96-well plates. Treatment was performed after 24 h with the indicated doses of archazolid for 72 h. In parallel SKBR3 cells were seeded as a two-dimensional culture and treated equally for 72 h. Cell viability was determined using the CellTiter-Glo Luminescent Cell Viability Kit (Promega) in a luminometer (Berthold Technologies).

Transelectronmicroscopy—SKBR3 cells were treated as indicated, and transelectronmicroscopy was carried out as described before (26).

Addition procedures are found in the supplemental Materials and Methods.

Statistics-All statistical analysis was performed using GraphPad Prism software. Error bars indicate S.E. All *t*-tests are two-tailed unpaired t tests. Time or dose courses were analyzed by two-way ANOVA.

#### **RESULTS**

Cytotoxic Effects of Archazolid—Archazolid induced apoptosis in breast cancer cell lines (SKBR3, MDA-MD-231, 4T1-Luc2) as well as in a pancreatic tumor cell line (L3.6pl) (Fig. 1A and supplemental Fig. 2S) in a dose- and time-dependent manner, and apoptotic cell death was confirmed by Hoechst staining (Fig. 1A). To this end, activation of caspase-3 and cleavage of PARP are shown (Fig. 1, *B* and *C*, and supplemental Fig. 2S). Apoptosis induction by archazolid is clearly caspase-dependent as preincubation of cells with the pan-caspase inhibitor QVD-OPh reduced the level of cell death to almost control level (Fig. 1D and supplemental Fig. 2S). Fig. 1E demonstrates that archazolid not only reduces viability of SKBR3 cells cultured in monolayers (two-dimensional culture) but also the viability of mammospheres (three-dimensional culture).

Increased Cytotoxicity of Archazolid toward Tumor Cells-Tumor cells are more sensitive to archazolid with respect to cytotoxicity and growth inhibition compared with nontumor cells. Archazolid (10 nm) induces approximately 30% apoptosis



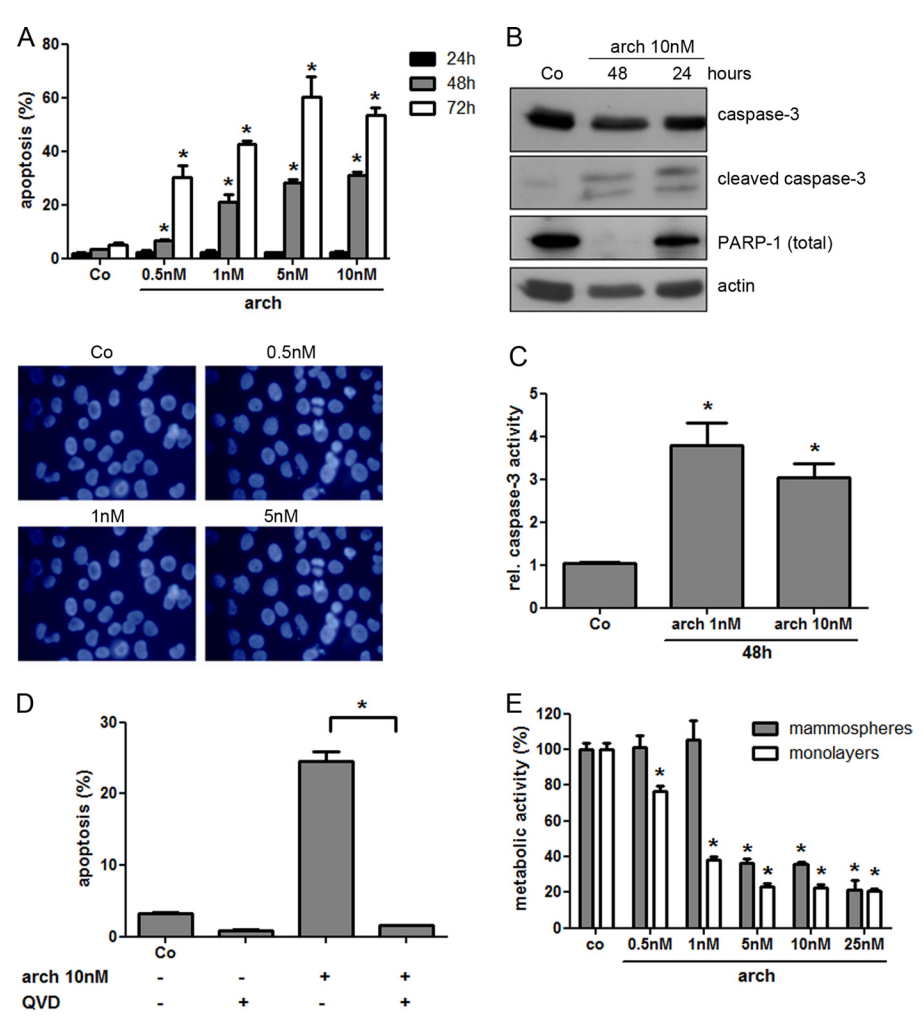


FIGURE 1. **Archazolid induces apoptosis in SKBR3 cells.** Cells were treated with increasing doses of archazolid (arch) or left untreated (Co) for increasing durations, and apoptosis induction was assessed by different methods. A, upper, cells with subdiploid nuclei were analyzed by propidium iodide staining followed by flow cytometry. Lower, apoptotic death was confirmed by staining cells with Hoechst 33258 ( $0.5~\mu g/ml$ ) after 48 h of archazolid treatment with different concentrations and confocal microscopy. B, cleavage of caspase-3 and PARP-1 was analyzed by Western blotting. C, enzymatic activity of caspase-3 was determined by cleavage of the fluorescing substrate DEVD-AFC. D, caspase dependence was assessed by pretreatment of the cells with 10  $\mu$ m pan-caspase inhibitor QVD-OPh for 1 h prior to archazolid treatment for 48 h followed by propidium iodide staining and flow cytometry. E, cytotoxic effects of archazolid on mammospheres were measured via metabolic activity. All experiments were performed at least three times in triplicate; \*,  $p \le 0.001$ . A, C, and E, ANOVA/Dunnett. D, Student's E test.

in SKBR3 cells but only 8% in nontumor MCF10A breast cells (Fig. 2A). Archazolid furthermore inhibits proliferation of mammary cancer cells (SKBR3) with an EC<sub>50</sub> of 0.013 nm and MCF10A with an EC50 of 0.12 nm (Fig. 2B). SKBR3 and MCF10A cells also responded differently to archazolid in a long term colony formation assay. Whereas SKBR3 cells treated with archazolid formed only 20% of the colonies counted in untreated cells, MCF10A cells still show approximately 50% survival (Fig. 2C). It is important to note that the extent of V-ATPase inhibition by archazolid was comparable in both cell types as shown by staining of lysosomes with a pH-sensitive fluorescence dye (LysoTracker) after incubation with increasing doses of archazolid for 2 h (Fig. 2D). Not only MCF10A cells were less sensitive, but also other tested nontumor cells (HEK293, L929, HUVECs, HMECs) showed less sensitivity concerning growth inhibition and apoptosis induction compared with a variety of tumor cells (SKBR3, L3.6pl, MCF-7, MDA-MB-231, 4T1-Luc2) (Fig. 2E and supplemental Fig. 2S).

Archazolid Induces the Intrinsic Apoptotic Pathway—The next step was to investigate the mode and mechanism of cell death conferred by archazolid treatment in more detail. (i) The mitochondrial potential was abrogated after 24 h of treatment with 1 as well as 10 nm archazolid as shown by an increased green fluorescence after JC-1 staining (Fig. 3A and supplemental Fig. 4S). (ii) An activation of the proapoptotic Bcl-2 family member Bax (Fig. 3B) as well as (iii) a release of cytochrome c and ROS from the mitochondria (Fig. 3C and supplemental Fig. 4S) and (iv) an activation of caspase-9 after 48 h of treatment (Fig. 3D) clearly point to the execution of archazolid-induced cell death by the intrinsic mitochondrial pathway. Interestingly, MCF10A cells also showed a slight decrease of the mitochondrial potential with 10 nm archazolid but not yet activation of caspase-9 (supplemental Fig. 4S). In contrast to the V-ATPase inhibitor concanamycin, archazolid does not directly damage mitochondria as shown in isolated rat liver mitochondria. Neither a decline in the mitochondrial membrane potential (Fig.

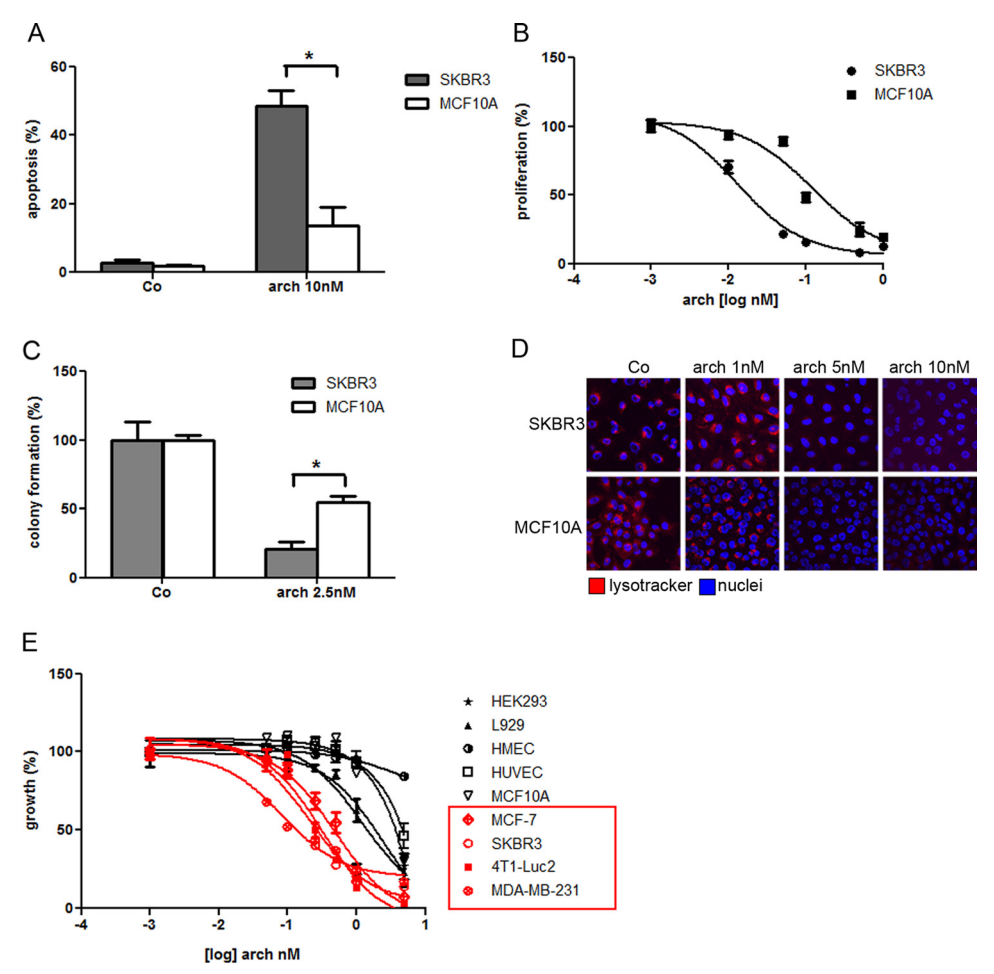


FIGURE 2. Tumor cells are more sensitive to archazolid. A and B, SKBR3 cells and the nontumor epithelial cell line MCF10A were treated with different concentrations of archazolid for (A) 48 h, and apoptosis was measured via propidium iodide staining and flow cytometry or (B) 72 h and proliferation was measured by crystal violet staining. C, for analysis of colony formation cells were treated with 2.5 nm archazolid for 24 h, trypsinized, and seeded at low density for 7 days, stained with crystal violet, and colonies were counted. Colonies of untreated control cells were set as 100%. D, for V-ATPase inhibition cells were treated for 2 h or left untreated (Co), and acidity of lysosomes was visualized using a pH-dependent LysoTracker and confocal microscopy. One representative picture of three independent sets is shown. E, growth inhibition of tumor and nontumor cells after archazolid treatment for 72 h and increasing doses was analyzed by CellTiter-Blue assay. \*,  $p \le 0.001$ , Student's t test.

3E) nor an elevated reactive oxygen species production or lowered ATP productivity was observed in the presence of archazolid, whereas a clear damage in such mitochondrial functions was induced by concanamycin (Fig. 3, E and F, and supplemental Fig. 4S).

Archazolid Induces the BH3-only Protein BNIP3-To get insight into signaling molecules and pathways affected by archazolid, a gene microarray of SKBR3 cells incubated with archazolid (1 and 10 nm) for 24 h has been performed. Genes regulated by archazolid belong to cell death, cellular growth/ differentiation, and in cancer-related pathways (supplemental Fig. 3S). One gene particularly up-regulated (2.7-fold and 3.5fold at 1 and 10 nm archazolid, respectively) was the BH3-only protein BNIP3 (supplemental Fig. 3S). These microarray data were confirmed on protein level (Fig. 4A). The expression of BNIP3 starts at 5 h after treatment and increases with time (48 h). Importantly, archazolid induced BNIP3 localized to the mitochondria as shown both by cell fractionation and Western blotting (Fig. 4B) as well as confocal microscopy (Fig. 4C). Along this line, it was interesting to see that BNIP3 heterodimerizes with Bcl-X<sub>L</sub> in cells treated with archazolid for

24 h, suggesting a role in mitochondrial apoptosis (Fig. 4D). As silencing BNIP3 does not abrogate apoptosis (Fig. 4E) BNIP3 in fact might rather be responsible for the reduced heterodimerization of Bcl-X<sub>I</sub> with beclin-1 observed in archazolid-treated cells (Fig. 4F), indicating an involvement of autophagy.

Role of Autophagy—Archazolid (10 nm) induces an accumulation of LC3II, a marker for autophagy, after 5 h as shown by confocal microscopy and Western blotting (Fig. 5A). Interestingly, the conversion of LC3I to LC3II and degradation of p62 occur at concentrations of archazolid that do not alkalize lysosomes but rather lead to an increased acidification (Fig. 5, B and C). At these low concentrations fusions of autophagosomes (EGFP-LC3) with lysosomes (Lamp-1) still occur, however, are inhibited at 10 nm archazolid (Fig. 5D). This points to an autophagy process that is actively induced by archazolid rather than caused by accumulation of autophagosomes, a process certainly occurring at higher concentrations of archazolid. In fact, electron microscopy was employed to confirm this notion. Double membrane vacuoles, i.e. autophagosomes, show up at 1 nm and 10 nm after 5 h of treatment. Huge multivesicular bodies



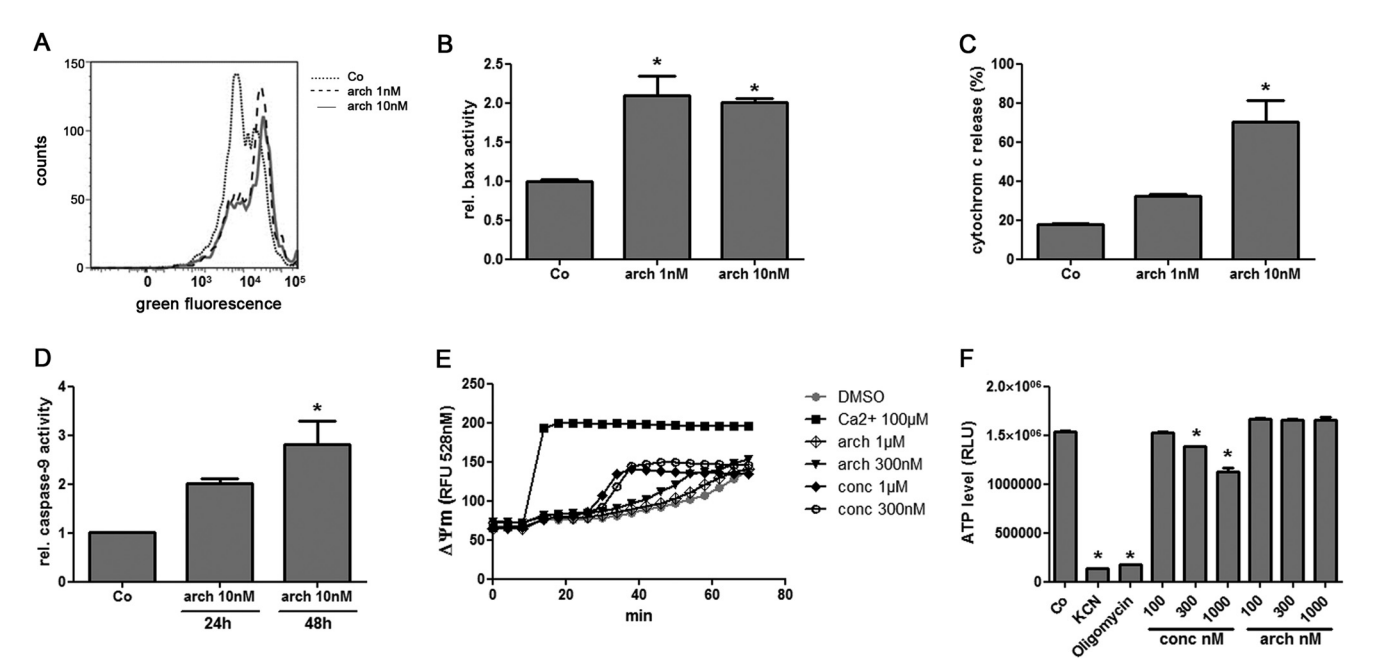


FIGURE 3. The mitochondrial pathway is induced by archazolid. A. SKBR3 cells were left untreated (dotted line) or incubated with 1 nm (solid line) and 10 nm (dashed line) archazolid for 24 h, and mitochondrial potential was assessed by JC-1 staining via flow cytometry. An increase in green fluorescence indicates the loss of membrane potential. B, the activation of Bax was measured by flow cytometry (anti-Bax 6A7) after 48 h of treatment. C, the release of cytochrome c from the mitochondria was measured via flow cytometry after 48 h. D, activation of caspase-9 was assessed by cleavage of LEHD-AFC via fluorometry after 24 and 48 h of treatment. E, mitochondrial membrane potential in rat liver mitochondrial suspensions was assessed by rhodamine-123 fluorescence. Increasing amounts of archazolid and concanamycin (conc) were tested; calcium served as positive control. F, ATP productivity was analyzed in isolated rat liver mitochondria after treatment with different concentrations of archazolid or concanamycin. Oligomycin and potassium cyanide (KCN) served as background controls. \*,  $p \le 0.05$ , ANOVA/Dunnett.

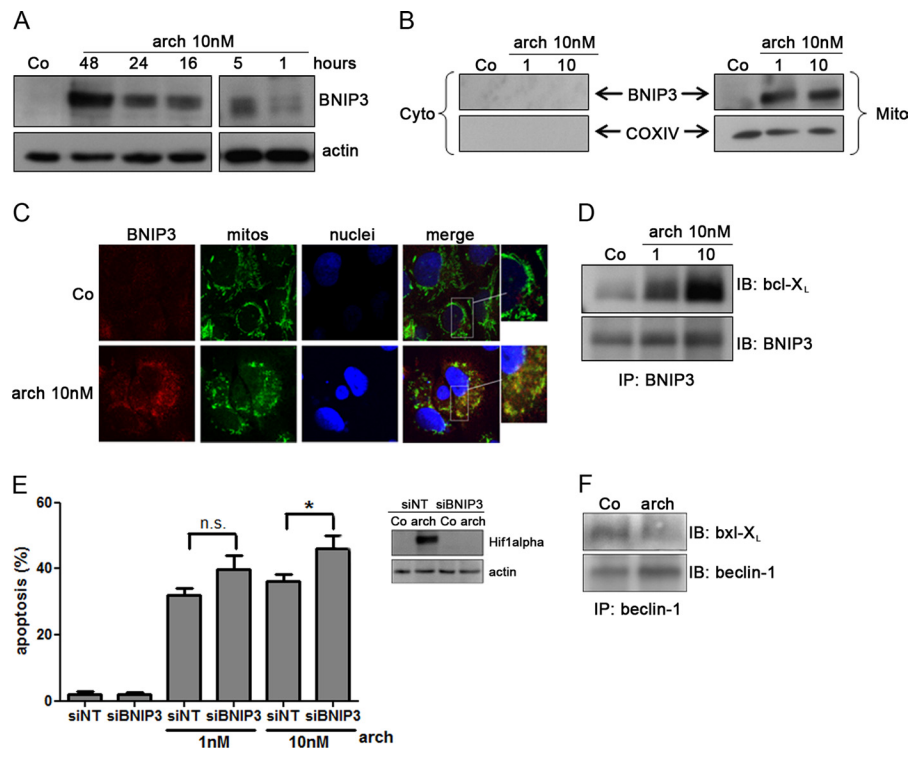


FIGURE 4. Archazolid induces BNIP3 expression. A, BNIP3 protein expression was analyzed in SKBR3 cells after different durations of archazolid (10 nm) treatment. B and C, BNIP3 induced by archazolid is found in the mitochondrial fraction (B) analyzed via Western blotting after cell fractionation or (C) confocal microscopy. Mitochondria were stained by MitoTracker (green) and BNIP3 by antibody (red). D, heterodimerization of BNIP3 with Bcl-X<sub>1</sub> is shown by immunoprecipitation (IP: BNIP3) after 24 h of archazolid treatment. E, BNIP3 was silenced using siRNA 24 h before archazolid treatment for 48 h, and apoptosis induction was determined by propidium iodide staining and flow cytometry. F, cells were treated with 10 nm archazolid for 24 h, and heterodimerization of beclin-1 with Bcl-X<sub>1</sub> was determined by immunoprecipitation IP, beclin-1. One representative experiment of three is shown. At least three independent experiments were performed. \*,  $p \le 0.05$ , Student's t test.

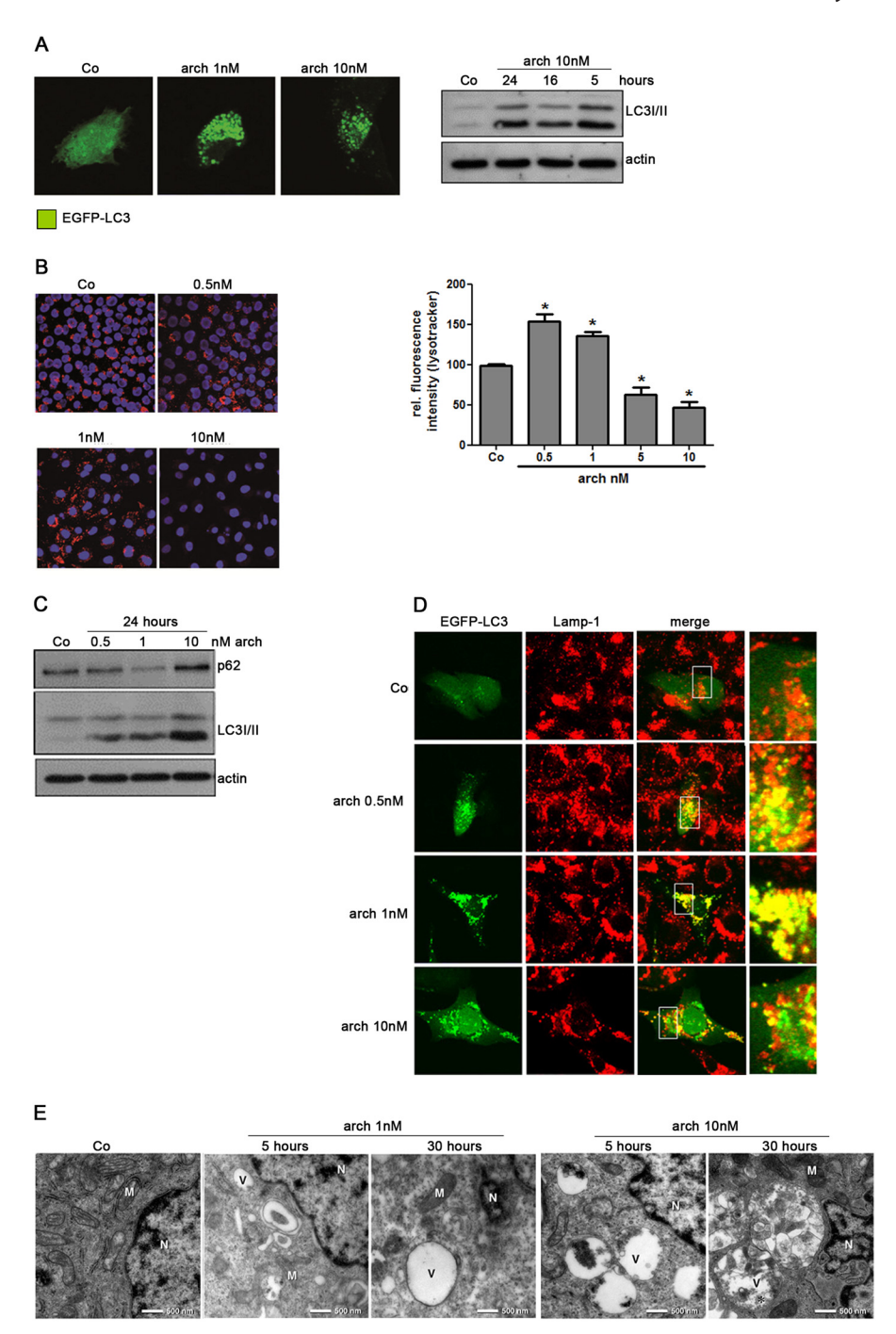


FIGURE 5. Archazolid induces autophagy. A, SKBR3 cells were transfected with EGFP-LC3, and LC3-positive vacuoles were examined via confocal microscopy or by conversion of LC3I to LC3II by Western blotting after different time points of archazolid (10 nm) treatment. B, cells were treated with increasing doses of archazolid for 24 h, and acidification of lysosomes was analyzed using a pH-dependent LysoTracker and confocal microscopy (left) or flow cytometry (right). C, conversion of LC3I to LC3II or expression of p62 at low concentrations was determined by Western blotting. D, fusion of autophagosomes with lysosomes was analyzed by transfecting cells with EGFP-LC3 and staining with Lamp-1 (lysosomes) via confocal microscopy after 24 h treatment with archazolid. E, archazolid-induced vacuoles (V) were analyzed by transelectronmicroscopy after treatment with 1 nm and 10 nm archazolid for 5 and 30 h. n, nucleus; M, mitochondria; \*, multivesicular bodies. Experiments are repeated three times. \*,  $p \le 0.05$ , ANOVA/Dunnett.

containing whole organelles appeared after 30 h upon treatment with 10 nm archazolid (Fig. 5E).

A next step was to analyze the role of autophagy in archazolid-induced cell death. Cells were pretreated with 3-methyladenine (3MA) which is an inhibitor of the autophagosome formation. Confocal microscopy and Western blot analysis in fact revealed the disappearance of LC3-positive vacuoles as well as the conversion of LC3I to LC3II (Fig. 6A). Z-sections of cells also showed that 3MA inhibited the swollen morphology which is caused by accumulating vacuoles in high dose (10 nm) archazolid-treated cells (Fig. 6B). Importantly, pretreatment of SKBR3 cells with 3MA significantly increased apoptosis induction at low concentrations of archazolid and reduced the apoptosis rate compared with treatment with archazolid alone at high concentrations (Fig. 6C). The knock-out of the specific autophagy-related gene ATG5 confirmed the effects shown for 3MA (Fig. 6D).

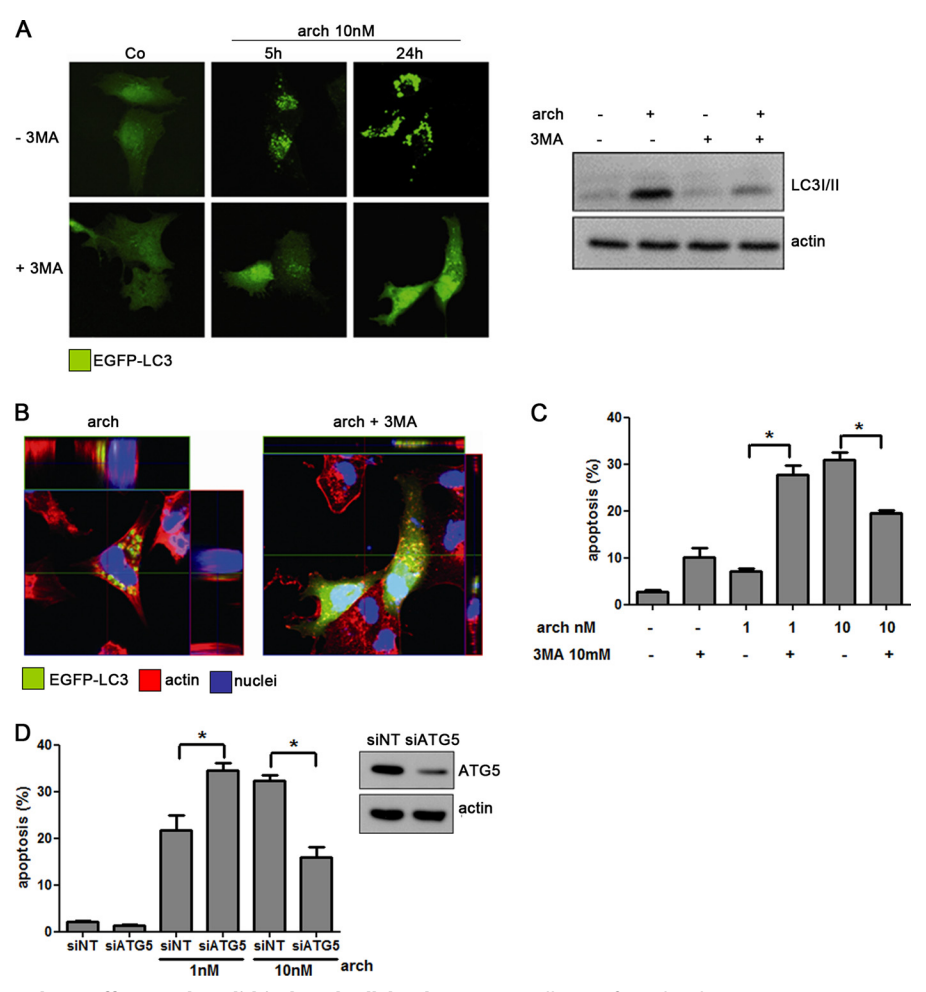


FIGURE 6. Inhibition of autophagy affects archazolid-induced cell death. A, SKBR3 cells transfected with EGFP-LC3 were pretreated with 10 mm 3MAbefore archazolid (10 nm) exposure, and (left) formation of autophagosomes or (right) conversion of LC3I to LC3II was analyzed by Western blotting. B, the morphology of the cell in a Z-section was analyzed by confocal microscopy. C, apoptosis induction after pretreatment with 3MA was assessed by propidium iodide staining and flow cytometry after 48 h. D, ATG5 was silenced using siRNA 24 h before archazolid treatment for 48 h, and apoptosis induction was determined by propidium iodide staining and flow cytometry. At least three independent experiments were performed;\*,  $p \le 0.05$ , Student's t test.

Archazolid Induces a Stress Response—Having found that archazolid induces a variety of stress responses, the next goal was to decipher the mechanism that actually mediates these responses and induces apoptosis. Reanalysis of the microarray data revealed many genes up-regulated by archazolid that are involved in glycolysis (supplemental Fig. 3S). Along this line, attention was paid to HIF1 $\alpha$ , the major inducer of glycolysis and also autophagy in hypoxia. Western blot analysis showed that archazolid strongly induced the expression of HIF1 $\alpha$  already at low concentrations. It was found in the cytosol as well as in the nucleus after 3 and 4 h, respectively (Fig. 7A). Furthermore, archazolid leads to an increased glucose uptake monitored by means of a fluorescent glucose analog, NBDG, which points to an activation of glycolysis also at lower concentrations of archazolid (Fig. 7B). Fig. 7C shows a decrease in ATP concentration after 3 h, which suggests that HIF1 $\alpha$  was activated due to energy stress. This notion was further supported by the activation of stress-sensing proteins such as the phosphorylation of the ATP/ADP ratio-sensing kinase AMPK and the translation initiation factor eIF2 $\alpha$  (Fig. 7D) as phosphorylation of these proteins inhibits energy-consuming processes. In addition, inhibition of P70S6K, an important readout of mTOR activity, has

been observed upon pharmacological V-ATPase inhibition (Fig. 7D). To analyze whether activation of HIF1 $\alpha$  is an adaptive mechanism to energy stress or involved in apoptosis induction, we silenced HIF1 $\alpha$  prior to archazolid treatment. We found that inhibiting the expression of HIF1 $\alpha$  increased the apoptosis-inducing capacities of archazolid, proposing the induction of HIF by archazolid as an escape mechanism (Fig. 7*E*).

As depicted in a schematic (Fig. 8), we sum up that inhibition of V-ATPase by archazolid leads to energy stress (ATP  $\downarrow$  , AMPK  $\uparrow$  , eIF2 $\alpha$   $\uparrow$  , P70S6K  $\downarrow$  ), which results in HIF1 $\alpha$  induction and autophagy. These processes are part of the cellular stress response and oppose apoptosis. Prolonged activation of these processes together with the blockage of  $H^+$  extrusion by V-ATPase inhibition finally ends up in mitochondrial apoptosis.

#### **DISCUSSION**

The present work characterized archazolid, a novel and highly potent pharmacological inhibitor of V-ATPases, as a promising experimental anticancer agent and demonstrates the potential of V-ATPase as a drugable target for tumor therapy. Mechanistic work gives insight into an interplay of apoptosis,



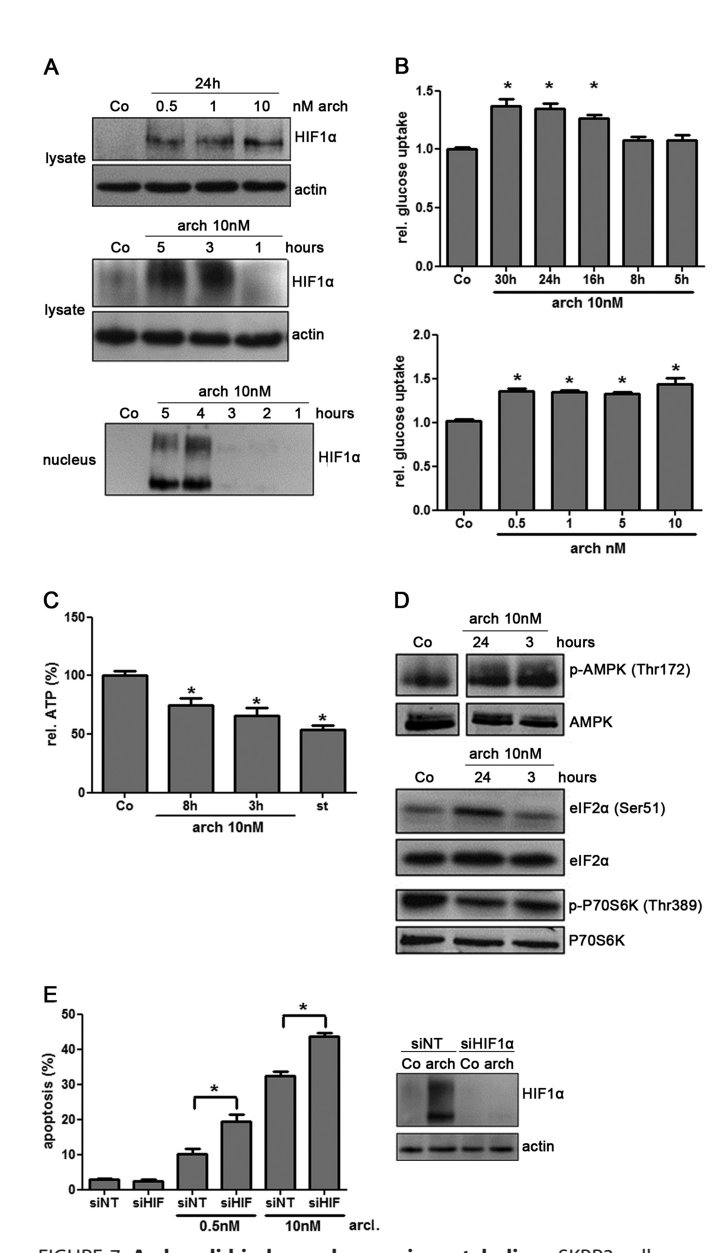


FIGURE 7. Archazolid induces changes in metabolism. SKBR3 cells were treated with different concentrations of archazolid for varying durations. A, expression of HIF1 $\alpha$  in the lysates or the nucleus was analyzed via Western blotting. B, cells were treated with archazolid (10 nm) for increasing durations or increasing concentrations (24 h) of archazolid, and glucose uptake was measured by flow cytometry using the fluorescing glucose analog NBDG. C, ATP concentration in the cells was measured after different durations of archazolid (10 nm) treatment or in starved (st) cells as a positive control. D, phosphorylation of P70S6K, AMPK, and elF2 $\alpha$  was analyzed by Western blotting after incubating the cells with 10 nm archazolid for 3 and 24 h. E, apoptosis was analyzed via propidium iodide staining and flow cytometry in cells transfected with siRNA against HIF1 $\alpha$  or control siRNA and treated with different concentrations of archazolid for 48 h. Experiments were repeated three times. \*,  $p \le 0.05$ . B and C, ANOVA/Dunnett; E, Student's t test.

autophagy, and cellular/metabolic stress in highly invasive tumor cells treated with archazolid.

Evidence is increasing that V-ATPase, an ubiquitous heteromultimeric proton pump, plays a role in cancer based on reports of increased expression and activity of the V-ATPase on the plasma membrane of tumor cells (1). Interestingly, invasive tumor cells show a different panel of a-subunit isoforms than noninvasive tumor cells. This is associated with the expression

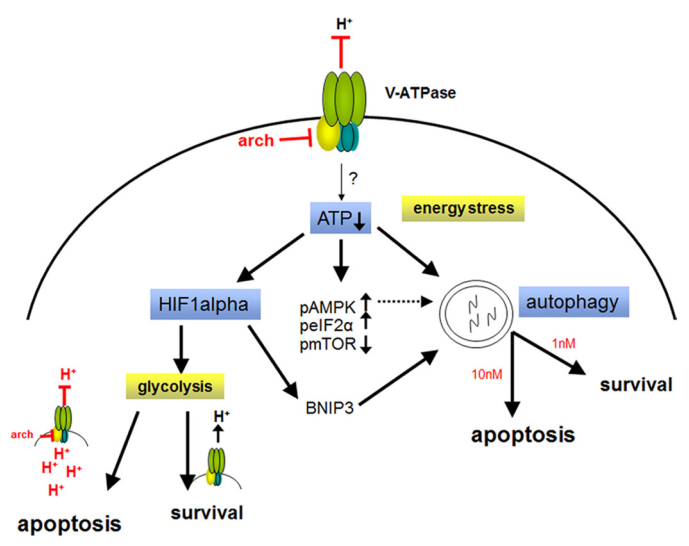


FIGURE 8. Schematic overview of V-ATPase inhibition and cell death. Inhibition of the V-ATPase by archazolid leads to a decrease of the ATP level and thereby to an activation of several stress responses like autophagy, HIF1 $\alpha$ induction, phosphorylation of the stress-sensing proteins AMPK and eIF2 $\alpha$ , and inhibition of mTOR. Autophagy serves as a survival process at low concentrations of archazolid but is involved in apoptosis induction at higher concentrations. HIF1 $\alpha$  leads to activation of glycolysis and BNIP3, which also leads to an induction of autophagy. Glycolysis serves as an escape mechanism in tumor cells; but due to defective pH regulation and inhibition of proton extrusion by archazolid, it leads to induction of apoptosis.

of the V-ATPase on the plasma membrane (27). The expression of the V-ATPase on the plasma membrane is also considered as a strategy of tumor cells to protect themselves from intracellular acidosis due to high metabolic activity and favors metastasis (1, 28). Remarkably, we did not observe a significant difference in V-ATPase expression (on mRNA as well as protein level) in a variety of breast tumor cells compared with nontumor breast epithelial cells in contrast to a report in pancreatic tumor (29). We however did find differences in a-subunit isoform distribution with SKBR3 cells showing a higher expression of the a3 isoform consistent with the data of Hinton et al. (supplemental Fig. 5S). Interestingly, all tested nontumor cells were significantly less sensitive toward V-ATPase inhibition by archazolid compared with SKBR3 breast carcinoma cells or a set of other tumor cells, an important fact also reported by Morimura et al. for normal liver cells in contrast to hepatoblastoma cells (8).

To this end, several V-ATPase inhibitors have been developed and investigated for their effects on cancer cells. There are reports showing that the long known V-ATPase inhibitors bafilomycin and concanamycin induce growth arrest and cell death in a variety of tumor cells (30), and more recently V-ATPase inhibitors like salicylihalamide (31) or NIK-12192 (32) have also been reported to possess antitumor activity. However, detailed information on the signaling pathways and molecular nodules used by these compounds is rather limited but crucial to understand the impact of pharmacological V-ATPase inhibition in cancer treatment.

Archazolids are a new group of V-ATPase inhibitors posing by their potency and selectivity (supplemental Fig. 1S) (3, 6). In fact, nanomolar concentrations of archazolid clearly induced apoptosis via caspase activation and the intrinsic pathway



which only partly applies to other V-ATPase inhibitors (7). Along this line, bafilomycin has shown to directly impair the functions of mitochondria (33), an effect we could not observe for archazolid on isolated rat liver mitochondria, but rather for concanamycin (Fig. 3, *E* and *F* and supplemental Fig. 4S). These differences suggest that archazolid possess higher specificity toward the V-ATPase compared with concanamycin and bafilomycin which could affect P-ATPases in mitochondria as secondary targets (34, 35). Gene array analysis of archazolid-treated cells further provided detailed information on signaling pathways affecting cell death and survival and highlighted a strong induction of BNIP3, a Bcl-2 family member and major player in cellular stress responses.

BNIP3 is known to induce caspase-dependent and -independent cell death via the mitochondria after receiving stress stimuli. However, BNIP3 has also prosurvival functions being involved in hypoxia-induced autophagy and death resistance (36–38).

BNIP3 induced by archazolid was found to be localized in the mitochondria and heterodimerized with  $\mathrm{Bcl-X_L}$  arguing in a first line for its role as mediator of intrinsic apoptosis induction. As genetic abrogation of BNIP3, however, did not lead to a reduction of cell death, BNIP3 activity is not crucial for apoptosis induction. It rather might be involved in autophagy by limiting the binding of beclin-1 and  $\mathrm{Bcl-X_L}$ .

In tumor cells, autophagy is mainly seen as a prosurvival process. It is activated under stress conditions such as nutrient starvation, hypoxia, and certain chemotherapeutics whereas prolonged autophagy can induce cell death (14-16).

V-ATPase inhibitors, which cause alkalization of lysosomes are often claimed to be autophagy inhibitors and used as experimental tools as autophagosomes accumulate due to impaired fusion with lysosomes (39). However, there are also reports showing that inhibition of autophagy is cell type-, concentration-, and time-dependent and cannot be generalized for V-ATPase inhibitors (40). Shacka *et al.* reported that low concentrations of bafilomycin do not lead to inhibition of autophagy despite alkalization of lysosomes (41), and Mousavi *et al.* did not observe an inhibition of fusion with autophagosomes and lysosomes at all (42).

In fact, archazolid leads to conversion of the autophagosome marker LC3I to LC3II at concentrations that do not lead to an alkalization, but even to an acidification of lysosomes (0.5 nm, 1 nm). At these concentrations, archazolid also leads to a degradation of p62, another autophagy marker, and a fusion of autophagosomes with lysosomes. This suggests that archazolid actually induces autophagy at low concentrations which cannot be accomplished at higher concentrations (10 nm) shown by accumulation of p62, impaired fusion of autophagosomes with lysosomes and cell swelling resulting from accumulating autophagosomes.

The question rises whether autophagy plays a role in archazolid-induced cell death. Inhibition of early stages of autophagy, *i.e.* inhibiting the formation of autophagosomes either by 3MA or by silencing *ATG5* was found to decrease cell death induced by archazolid at high concentrations, but leads to an increase of cell death at low concentrations of the drug

supporting a protective role of autophagy induction which opposes apoptotic activity of archazolid.

What is the cause of autophagy and BNIP3 induction by archazolid? The microarray shows an induction of glycolysisrelated genes normally up-regulated under hypoxia (supplemental Fig. 3S). In fact, archazolid treatment leads to a decreased ATP level followed by a strong induction of HIF1 $\alpha$ , which is activated under hypoxic stress, as well as an increase of glucose uptake. HIF induction by the V-ATPase inhibitor bafilomycin was also described by Lim et al., suggesting a role in growth inhibition and showing a translocation of the c-subunit with HIF1 $\alpha$  to the nucleus (43). We did not observe this effect after archazolid treatment (data not shown) possibly due to a slightly different binding mode of archazolid on the c-subunit (6, 44). In parallel, by inhibiting mTOR activity, and thus P70S6K, and stimulating phosphorylation of the energy-sensing kinase AMPK and the initiation of translation factor eIF2 $\alpha$ , archazolid shuts down energy-consuming processes like proliferation, translation, or fatty acid synthesis (46, 47). Interestingly, a recent paper by the group of Sabatini et al. identified V-ATPase as a component of the mTOR pathway important for lysosomal amino acid sensing (48).

Although invasive tumor cells often have an altered metabolism and a constitutive active HIF1 $\alpha$  we did not find constitutive HIF1 $\alpha$  expression in SKBR3 cells as is the case for some other invasive tumor cells (45). Interestingly, archazolid induces HIF1 $\alpha$  also in nontumor cells (data not shown). However, as normal cells do have a lower proliferation rate and a far lower metabolic flux, energy stress might have a smaller impact on normal cells, which leaves them less sensitive toward V-AT-Pase expression.

Our data suggest that, as described in Fig. 8, cells treated with archazolid run into energy stress shown by a decline of the ATP level. To cope with this a cellular stress response is induced with induction of autophagy and HIF1 $\alpha$ . These processes are succeeded by BNIP3 activation and a shutdown of energy-consuming processes trying to escape cell death. But prolonged activation of these processes will eventually lead to apoptosis induction, especially when proton transport is disturbed as is the case via V-ATPase inhibition. As silencing HIF1 $\alpha$  leads to increased apoptosis in archazolid-treated cells, this consumption is confirmed.

Archazolid is certainly an interesting tool to decipher the role of V-ATPase as a target at the interplay of apoptosis, autophagy, and tumor cell metabolism. Interfering with these stress responses could surely be a future perspective to increase archazolid-induced apoptosis as already shown for silencing ATG5 and HIF1 $\alpha$ .

Acknowledgments—We thank Bernadette Grohs and Lina Schneider for excellent work.

#### **REFERENCES**

- Forgac, M. (2007) Vacuolar ATPases: rotary proton pumps in physiology and pathophysiology. Nat. Rev. Mol. Cell Biol. 8, 917–929
- Sennoune, S. R., Bakunts, K., Martínez, G. M., Chua-Tuan, J. L., Kebir, Y., Attaya, M. N., and Martínez-Zaguilán, R. (2004) Vacuolar H<sup>+</sup>-ATPase in human breast cancer cells with distinct metastatic potential:



- distribution and functional activity. Am. J. Physiol. Cell Physiol. 286, C1443-1452
- 3. Huss, M., Vitavska, O., Albertmelcher, A., Bockelmann, S., Nardmann, C., Tabke, K., Tiburcy, F., and Wieczorek, H. (2011) Vacuolar H<sup>+</sup>-ATPases: intra- and intermolecular interactions. Eur. J. Cell Biol. 90, 688-695
- 4. Roethle, P. A., Chen, I. T., and Trauner, D. (2007) Total synthesis of (-)archazolid B. J. Am. Chem. Soc. 129, 8960 - 8961
- 5. Menche, D., Hassfeld, J., Li, J., and Rudolph, S. (2007) Total synthesis of archazolid A. J. Am. Chem. Soc. 129, 6100-6101
- 6. Bockelmann, S., Menche, D., Rudolph, S., Bender, T., Grond, S., von Zezschwitz, P., Muench, S. P., Wieczorek, H., and Huss, M. (2010) Archazolid A binds to the equatorial region of the c-ring of the vacuolar H<sup>+</sup>-ATPase. J. Biol. Chem. 285, 38304-38314
- 7. Nakashima, S., Hiraku, Y., Tada-Oikawa, S., Hishita, T., Gabazza, E. C., Tamaki, S., Imoto, I., Adachi, Y., and Kawanishi, S. (2003) Vacuolar H+-ATPase inhibitor induces apoptosis via lysosomal dysfunction in the human gastric cancer cell line MKN-1. J. Biochem. 134, 359-364
- 8. Morimura, T., Fujita, K., Akita, M., Nagashima, M., and Satomi, A. (2008) The proton pump inhibitor inhibits cell growth and induces apoptosis in human hepatoblastoma. Pediatr. Surg. Int. 24, 1087-1094
- 9. De Milito, A., Iessi, E., Logozzi, M., Lozupone, F., Spada, M., Marino, M. L., Federici, C., Perdicchio, M., Matarrese, P., Lugini, L., Nilsson, A., and Fais, S. (2007) Proton pump inhibitors induce apoptosis of human B-cell tumors through a caspase-independent mechanism involving reactive oxygen species. Cancer Res. 67, 5408 -5417
- 10. Kültz, D. (2005) Molecular and evolutionary basis of the cellular stress response. Annu. Rev. Physiol. 67, 225-257
- 11. Fulda, S., Gorman, A. M., Hori, O., and Samali, A. (2010) Cellular stress responses: cell survival and cell death. Int. J. Cell Biol. 2010, 214074
- 12. Burton, T. R., and Gibson, S. B. (2009) The role of Bcl-2 family member BNIP3 in cell death and disease: NIPping at the heels of cell death. Cell Death Differ. 16, 515-523
- 13. Bellot, G., Garcia-Medina, R., Gounon, P., Chiche, J., Roux, D., Pouysségur, J., and Mazure, N. M. (2009) Hypoxia-induced autophagy is mediated through hypoxia-inducible factor induction of BNIP3 and BNIP3L via their BH3 domains. Mol. Cell. Biol. 29, 2570-2581
- 14. Tschan, M. P., and Simon, H. U. (2010) The role of autophagy in anticancer therapy: promises and uncertainties. J. Intern. Med. 268, 410-418
- 15. Kroemer, G., and Levine, B. (2008) Autophagic cell death: the story of a misnomer. Nat. Rev. Mol. Cell Biol. 9, 1004-1010
- 16. Amelio, I., Melino, G., and Knight, R. A. (2011) Cell death pathology: cross-talk with autophagy and its clinical implications. Biochem. Biophys. Res. Commun. 414, 277-281
- 17. Majmundar, A. J., Wong, W. J., and Simon, M. C. (2010) Hypoxiainducible factors and the response to hypoxic stress. Mol. Cell 40,
- 18. Kubasiak, L. A., Hernandez, O. M., Bishopric, N. H., and Webster, K. A. (2002) Hypoxia and acidosis activate cardiac myocyte death through the Bcl-2 family protein BNIP3. Proc. Natl. Acad. Sci. U.S.A. 99,
- 19. Greijer, A. E., and van der Wall, E. (2004) The role of hypoxia inducible factor 1 (HIF-1) in hypoxia-induced apoptosis. J. Clin. Pathol. 57, 1009 - 1014
- 20. Nicoletti, I., Migliorati, G., Pagliacci, M. C., Grignani, F., and Riccardi, C. (1991) A rapid and simple method for measuring thymocyte apoptosis by propidium iodide staining and flow cytometry. J. Immunol. Methods 139, 271-279
- 21. Schneiders, U. M., Schyschka, L., Rudy, A., and Vollmar, A. M. (2009) BH3-only proteins Mcl-1 and Bim as well as endonuclease G are targeted in spongistatin 1-induced apoptosis in breast cancer cells. Mol. Cancer Ther. 8, 2914-2925
- 22. Waterhouse, N. J., and Trapani, J. A. (2003) A new quantitative assay for cytochrome c release in apoptotic cells. Cell Death Differ. 10, 853 - 855
- 23. Petit, P. X., Goubern, M., Diolez, P., Susin, S. A., Zamzami, N., and Kroemer, G. (1998) Disruption of the outer mitochondrial membrane as a result of large amplitude swelling: the impact of irreversible permeability transition. FEBS Lett. 426, 111-116

- 24. Zamzami, N., Métivier, D., and Kroemer, G. (2000) Quantitation of mitochondrial transmembrane potential in cells and in isolated mitochondria. Methods Enzymol. **322**, 208 – 213
- 25. Dirsch, V. M., Stuppner, H., and Vollmar, A. M. (2001) Helenalin triggers a CD95 death receptor-independent apoptosis that is not affected by overexpression of Bcl-X<sub>1</sub> or Bcl-2. Cancer Res. **61**, 5817–5823
- 26. López-Antón, N., Hermann, C., Murillo, R., Merfort, I., Wanner, G., Vollmar, A. M., and Dirsch, V. M. (2007) Sesquiterpene lactones induce distinct forms of cell death that modulate human monocyte-derived macrophage responses. Apoptosis 12, 141-153
- 27. Hinton, A., Sennoune, S. R., Bond, S., Fang, M., Reuveni, M., Sahagian, G. G., Jay, D., Martinez-Zaguilan, R., and Forgac, M. (2009) Function of a subunit isoforms of the V-ATPase in pH homeostasis and in vitro invasion of MDA-MB231 human breast cancer cells. J. Biol. Chem. 284,
- 28. Lagadic-Gossmann, D., Huc, L., and Lecureur, V. (2004) Alterations of intracellular pH homeostasis in apoptosis: origins and roles. Cell Death Differ. 11, 953-961
- 29. Ohta, T., Numata, M., Yagishita, H., Futagami, F., Tsukioka, Y., Kitagawa, H., Kayahara, M., Nagakawa, T., Miyazaki, I., Yamamoto, M., Iseki, S., and Ohkuma, S. (1996) Expression of 16 kDa proteolipid of vacuolar-type H<sup>+</sup>-ATPase in human pancreatic cancer. Br. J. Cancer 73, 1511–1517
- 30. Wu, Y. C., Wu, W. K., Li, Y., Yu, L., Li, Z. J., Wong, C. C., Li, H. T., Sung, J. J., and Cho, C. H. (2009) Inhibition of macroautophagy by bafilomycin A1 lowers proliferation and induces apoptosis in colon cancer cells. Biochem. Biophys. Res. Commun. 382, 451-456
- 31. Lebreton, S., Jaunbergs, J., Roth, M. G., Ferguson, D. A., and De Brabander, J. K. (2008) Evaluating the potential of vacuolar ATPase inhibitors as anticancer agents and multigram synthesis of the potent salicylihalamide analog saliphenylhalamide. Bioorg. Med. Chem. Lett. 18, 5879-5883
- 32. Supino, R., Petrangolini, G., Pratesi, G., Tortoreto, M., Favini, E., Bo, L. D., Casalini, P., Radaelli, E., Croce, A. C., Bottiroli, G., Misiano, P., Farina, C., and Zunino, F. (2008) Antimetastatic effect of a small-molecule vacuolar H<sup>+</sup>-ATPase inhibitor in *in vitro* and *in vivo* preclinical studies. *J. Pharma*col. Exp. Ther. **324**, 15–22
- 33. Teplova, V. V., Tonshin, A. A., Grigoriev, P. A., Saris, N. E., and Salkinoja-Salonen, M. S. (2007) Bafilomycin A1 is a potassium ionophore that impairs mitochondrial functions. J. Bioenerg. Biomembr. 39, 321-329
- 34. Huss, M., Sasse, F., Kunze, B., Jansen, R., Steinmetz, H., Ingenhorst, G., Zeeck, A., and Wieczorek, H. (2005) Archazolid and apicularen: novel specific V-ATPase inhibitors. BMC Biochem. 6, 13
- 35. Dröse, S., and Altendorf, K. (1997) Bafilomycins and concanamycins as inhibitors of V-ATPases and P-ATPases. J. Exp. Biol. 200, 1-8
- 36. Zhang, J., and Ney, P. A. (2009) Role of BNIP3 and NIX in cell death, autophagy, and mitophagy. Cell Death Differ. 16, 939-946
- 37. Mellor, H. R., and Harris, A. L. (2007) The role of the hypoxia-inducible BH3-only proteins BNIP3 and BNIP3L in cancer. Cancer Metastasis Rev. **26,** 553–566
- 38. Cosse, J. P., Rommelaere, G., Ninane, N., Arnould, T., and Michiels, C. (2010) BNIP3 protects HepG2 cells against etoposide-induced cell death under hypoxia by an autophagy-independent pathway. Biochem. Pharmacol. 80, 1160-1169
- 39. Yamamoto, A., Tagawa, Y., Yoshimori, T., Moriyama, Y., Masaki, R., and Tashiro, Y. (1998) Bafilomycin A1 prevents maturation of autophagic vacuoles by inhibiting fusion between autophagosomes and lysosomes in rat hepatoma cell line, H-4-II-E cells. Cell Struct. Funct. 23, 33-42
- 40. Fass, E., Shvets, E., Degani, I., Hirschberg, K., and Elazar, Z. (2006) Microtubules support production of starvation-induced autophagosomes but not their targeting and fusion with lysosomes. J. Biol. Chem. 281, 36303-36316
- 41. Shacka, J. J., Klocke, B. J., Shibata, M., Uchiyama, Y., Datta, G., Schmidt, R. E., and Roth, K. A. (2006) Bafilomycin A1 inhibits chloroquine-induced death of cerebellar granule neurons. Mol. Pharmacol. 69, 1125-1136
- 42. Mousavi, S. A., Kjeken, R., Berg, T. O., Seglen, P. O., Berg, T., and Brech, A. (2001) Effects of inhibitors of the vacuolar proton pump on hepatic heterophagy and autophagy. Biochim. Biophys. Acta 1510, 243-257
- 43. Lim, J. H., Park, J. W., Kim, S. J., Kim, M. S., Park, S. K., Johnson, R. S., and Chun, Y. S. (2007) ATP6V0C competes with von Hippel-Lindau protein in



- hypoxia-inducible factor  $1\alpha$  (HIF- $1\alpha$ ) binding and mediates HIF- $1\alpha$  expression by bafilomycin A1. Mol. Pharmacol. 71, 942-948
- 44. Wang, Y., Inoue, T., and Forgac, M. (2005) Subunit a of the yeast V-ATPase participates in binding of bafilomycin. J. Biol. Chem. 280, 40481 - 40488
- 45. Semenza, G. (2002) Signal transduction to hypoxia-inducible factor 1. Biochem. Pharmacol. 64, 993-998
- 46. Wek, R. C., Jiang, H. Y., and Anthony, T. G. (2006) Coping with stress: eIF2 kinases and translational control. Biochem. Soc. Trans. 34, 7-11
- 47. Luo, Z., Zang, M., and Guo, W. (2010) AMPK as a metabolic tumor suppressor: control of metabolism and cell growth. Future Oncol. 6, 457–470
- 48. Zoncu, R., Bar-Peled, L., Efeyan, A., Wang, S., Sancak, Y., and Sabatini, D. M. mTORC1 senses lysosomal amino acids through an inside-out mechanism that requires the vacuolar H<sup>+</sup>-ATPase. Science 334, 678 – 683